N-Heterocyclic Carbene-Based Iridium and Ruthenium/Iridium Nanoparticles for the Hydrogen Isotope Exchange Reaction through C–H Bond Activations

Alejandra Zuluaga-Villamil, Gabriel Mencia, Juan M Asensio, Pier-Francesco Fazzini, Edwin A Baquero, Bruno Chaudret

N-Heterocyclic Carbene-based Iridium and Ruthenium/Iridium Nanoparticles for Hydrogen Isotope Exchange Reaction Through C–H Bond Activations

Alejandra Zuluaga-Villamil,[a] Gabriel Mencia,*[b] Juan M. Asensio,[b†] Pier-Francesco Fazzini,[b] Edwin A. Baquero,*[a] and Bruno Chaudret*[b]

[a] Estado Sólido y Catálisis Ambiental (ESCA), Departamento de Química, Facultad de Ciencias, Universidad Nacional de Colombia, Carrera 30 No. 45-03, 111321, Bogotá, Colombia.

[b] LPCNO, Laboratoire de Physique et Chimie de Nano-Objets, UMR, 5215 INSA-CNRS-UPS, Institut National des Sciences Appliques 135, Avenue de Rangueil, 31077, Toulouse, France.

KEYWORDS: Ruthenium, Iridium, Bimetallic, Hydrogen Isotope Exchange, Nanoparticles, N-Heterocyclic Carbenes

ABSTRACT: Suppressing aromatic rings reduction in noble-metal catalyzed H/D exchange reactions still remains a challenge. This drawback may be overcome by finding a synergetic effect in bimetallic nanoparticles (NPs). Herein we report the synthesis of bimetallic lipo- and water-soluble Ru/Ir NPs. They were characterized by state-of-the-art techniques such as TEM, HR-TEM, ATR-FTIR, XRD, and solid-state NMR. These NPs were found to be dispersible in both organic and aqueous media thanks to the stabilization and coordination of adequate N-Heterocyclic Carbene (NHC) ligands to the NP surface. They were tested in the deuteration of 2-phenylpyridine, 2-methyl-naftylamine, 5,6,7,8-tetrahydro-naftylamine, and L-lysine using D_2 as isotopic source. Bimetallic NPs showed an unusual selectivity towards the H/D exchange of 2-phenylpyridine, deuterating not only the expected C–H positions close to the N atom, but also remote positions on the heterocycle. Additionally, reduction of the aromatic rings, which is a common undesired side-reaction catalyzed by Ru NPs, was not observed. These outcomes, rationalised by a synergetic effect of both metals, are enhanced when NHC ligands are on the surface in comparison to model catalysts stabilized by polyvinylpyrrolidone (PVP). Concerning non-aromatic substrates, CH_2-α and CH_2-ε positions to the amino acid group of L-lysine were fully deuterated, while moderate deuteration of γ position was observed as iridium content was increased in the bimetallic system.

INTRODUCTION

The interaction of transition metals with C–H bonds has been one of the important topics studied by Maurice Brookhart. His seminal paper with Malcolm Green on agostic interactions has initiated a considerable development of research in this area[1–3] Although the mechanistic studies on C–H activation were first concentrated on molecular species, the development of organometallic nanoparticles accommodating hydrides at their surface was a clear extension of these early works.

Furthermore, besides being a clear proof of C–H activation, the hydrogen isotope exchange (HIE) reaction is of importance for various fields and first the development of life sciences.[4–7] Thus, deuterated molecules may be applied as internal standards for mass spectrometry[8] or for mechanistic studies in organic and organometallic chemistry.[4] The use of C–H bond activations for HIE is a direct methodology that enables the synthesis of deuterated molecules in a straightforward fashion. Nowadays, several noble-metal such as Ir,[9] Ru,[10,11] Rh,[12,13] Pd or Pt[11] can catalyse this reaction in homogeneous phase, as well as some non-noble metals (Fe, Co, Ni).[14,15] In addition, heterogeneous catalysts such as Pd@C, Pt@C, Ru@C,[11] and Ni[16,17] have also been found active in this catalytic process. During the last years, the use of mono- and bi-metallic nanoparticles (NPs) in HIE has emerged as a promising tool, since NPs have proven to be very efficient and selective catalysts for this reaction.[18] This is due the possibility of modulating their size, shape, and composition, allowing control on their reactivity.[19] In this sense, some of us have reported the use of Ru NPs for the selective deuteration of several nitrogen and sulfur containing bioactive compounds.[20,21] Afterwards, this protocol has been extended to the enantiospecific deuteration of a large diversity of amino acids.[22] Nevertheless, if the protocol is extended to aromatic substrates, Ru NPs display a major drawback because of their high activity in reduction of these substrates.[23,24] In contrast, the functionalization of NPs with organic ligands permits not only to stabilize them in the reaction medium, but also to tune the solubility, selectivity, and catalytic activity, which can constitute a great advantage over conventional heterogeneous catalysts.[25] In this sense, *N*-Heterocyclic Carbene (NHC) ligands have emerged as versatile NPs stabilizers due to their unique stereoelectronic properties.[26–30] Thus, we reported the synthesis of water-soluble NHC-stabilized Ru NPs that

were able to deuterate successfully the CH_2-α, CH_2-γ, and CH_2-ε positions to the amino-acid moiety at pHs higher than 10.[31] However, the reduction of aromatic substrates using monometallic Ru NPs functionalized by NHCs still persists.[30] On the other hand, Ir NPs have been shown to be a highly selective metal for H/D exchange, suppressing the reduction of aromatic systems in the deuteration of anilines,[32] affording a non-conventional selectivity but moderate activity. In this sense, synergistic effects may appear in bimetallic systems when two metals combine their beneficial properties in catalytic processes. Thus, some of us have been interested in tailor-made bimetallic NPs for tuning the chemical and physical properties of the systems. For example, Ru/Pt NPs have been synthesized with different stabilizers such as polyvinylpyrrolidone (PVP),[33–35] or 1,4-bis(diphenylphosphino)butane (dppb)[36] and the influence of the chemical order within these particles on their reactivity has been evidenced. Regarding HIE reactions, we recently reported the first water-soluble Ru/Pt NPs stabilized by NHCs for the selective deuteration of L-lysine. It allowed us to improve the selectivity respect to pure Ru NPs while maintaining good catalytic activites.[37] Although Ru/Ir bimetallic catalysts have been reported for hydrodehalogenation reaction,[38] hydrogenation of 5-hydroxymethylfurfural,[39] and levulinic acid,[40] reduction of NOx by CO,[41] and evolution of oxygen in acidic environments,[42] there are no reports in HIE. Thus, the use of bimetallic Ru/Ir NPs in this process might then be of interest to overcome the reduction issue.

Herein, we report the synthesis of novel bimetallic Ru/Ir NPs stabilized by NHC ligands to study their synergistic behavior in H/D exchange reactions of nitrogenous aromatic molecules. The NPs were successfully characterized by state-of-the-art techniques. Their bimetallic nature was confirmed by means of High Resolution-Transmission Electron Microscopy (HR-TEM) coupled to Energy Dispersive X-Ray (EDX) spectroscopy. The bimetallic NPs were able to deuterate nitrogenous aromatic compounds without reducing the aromatic ring, displaying a beneficial synergistic effect between both metals. An electronic effect in the bimetallic systems caused by NHC ligands is also presented when comparing with their counterparts stabilized by PVP.

RESULTS AND DISCUSSION

Synthesis and Characterization of Nanoparticles

Monometallic Ru (**Ru**) and Ir (**Ir**) NPs were synthesized by decomposition of [Ru(COD)(COT)] (COD = 1,5-Cyclooctadiene; COT = 1,3,5-cyclooctatriene) and $[IrOMe(COD)_2]_2$, respectively according to previously reported protocols using polyvinylpyrrolidone (PVP) or NHCs as stabilizers.[24-31,32] Briefly, the reactions were carried out in THF at room temperature (r.t.) under H_2 pressure (3 bar) during 24h. In order to study the effect of both metals in H/D exchange reactions, bimetallic NPs were prepared by co-decomposition of both precursors, using a Ru:Ir molar ratio of 1:2 (**$RuIr_2$**) and 2:1 (**Ru_2Ir**). All NPs were stabilized by polyvinylpyrrolidone (**PVP**, 5 wt%) or the corresponding NHCs (0.2 equiv) namely 1,3-bis-(2,4,6-trimethylplhenyl) imidazolium-2-ylidene (**IMes**) and 1-(2,4,6-trimethylphenyl)-3-(3-potassium sulfonate-propyl)-imidazol-2-ylidene (**$IMesPrSO_3$**) (Scheme 1). These NHCs were previously formed by deprotonation of the imidazolium salts with KO^tBu (See Supporting Information for details). The resulting lipo- and water-soluble nanoparticles obtained were obtained as black powders after purification. Transmission electron microscopy (TEM) analyses of **Ru** and **Ir** NPs stabilized with PVP (**Ru@PVP**; **Ir@PVP**), IMes (**Ru@IMes**; **Ir@IMes**), and $IMesPrSO_3$ (**Ru@$IMesPrSO_3$**; **Ir@$IMesPrSO_3$**) exhibited ultra-small spherical, well-distributed and monodispersed NPs with diameters ranging between 1.1 and 1.3 nm (Figures 1a, 1b, S3, S4, S7, and S8, for **Ru@IMes**, **Ir@IMes**, **Ru@PVP**, **Ir@PVP**, **Ru@$IMesPrSO_3$**, and **Ir@$IMesPrSO_3$**, respectively). These values are comparable to those previously reported for ruthenium and iridium nanoparticles functionalized by similar ligands.[22,43] The bimetallic NPs do not differ significantly in size from their monometallic analogues ranging from 1.1 to 1.7 nm as observed in Figures 1c, 1d, S5, S6, S9, and S10, for **Ru_2Ir@IMes**, **$RuIr_2$@IMes**, **$RuIr_2$@PVP**, **Ru_2Ir@PVP**, **$RuIr_2$@$IMesPrSO_3$**, and **Ru_2Ir@$IMesPrSO_3$**, respectively. It should be noted that the colloidal stability of the NHC-stabilized systems is much better than those stabilized by PVP, which show metallic deposition after 3 days. Instead, lipo and water-soluble NHC-stabilized NPs were found to be dispersible and to give rise to stable colloidal solutions for months in organic solvents (e.g. toluene, THF, acetone) and water, respectively.

Scheme 1. Synthesis of Ru, Ir, and Ru/Ir NPs.

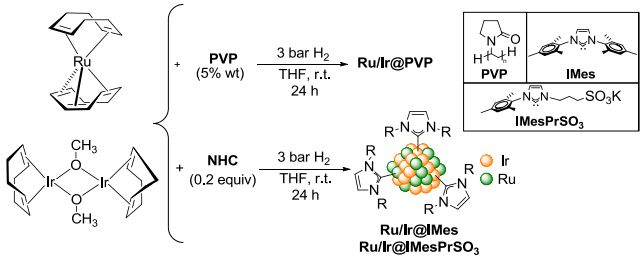

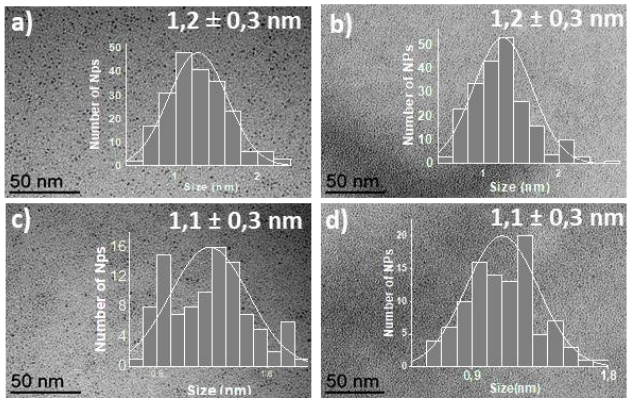

Figure 1. TEM pictures for a) **Ru@IMes**, b) **Ir@IMes**, c)**Ru_2Ir@IMes,** and d) **$RuIr_2$@IMes**.

Powder X-Ray Diffraction (XRD) analyses for **Ru@IMes**, and **Ir@IMes** are crystalline and display the hexagonal close-packed (hcp) and the face centered cubic (fcc) structures of Ru and Ir, respectively (Figures S11, and S12). In

the bimetallic systems both hcp and fcc structures can be observed (Figures S13, and S14 for **Ru_2Ir@IMes**, and **$RuIr_2$@IMes**, respectively). Similar results were obtained for NPs stabilized by **$IMesPrSO_3$** ligand (Figures S15–S17). However, we were not able to calculate the crystallite size in these samples because of the ultra-small sizes of the obtained nanoparticles.

With the aim to verify the bimetallic nature of the NPs, High-Resolution Scanning Transmission Electron Microscopy (STEM) studies were carried out on the samples **$RuIr_2$@IMes** and **Ru_2Ir@IMes**. High Resolution STEM in bright field (BF) and high-angle annular dark-field (HAADF), obtained with an atomic resolution microscope (ARM) showed that **Ru_2Ir@IMes** and **$RuIr_2$@IMes** are mainly monocrystalline (Figure 2). The crystalline structure could not be determined due to the fragmentation and shape change of the NPs under the electron beam. Nevertheless, Energy-dispersive X-ray spectroscopy (EDX) confirmed the presence of Ru/Ir NPs with atomic ratio of 70:30 and 36:64 for **Ru_2Ir@IMes** and **$RuIr_2$@IMes**, respectively. This result is in agreement with the ratio expected for both samples and the formation of bimetallic Ru/Ir NPs.

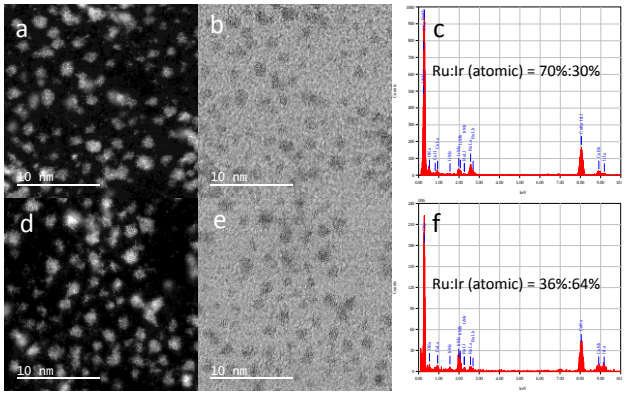

Figure 2. High-resolution STEM HAADF, BF image and relative composition determined by EDX of **Ru_2Ir@IMes** (a, b, and c, respectively) and **$RuIr_2$@IMes** (d, e, and f, respectively). For a better legibility, Figures 2c and 2f are also in the Supporting Information as Figures S9 and S10, respectively.

Surface Studies

In order to study the surface state of the NPs, Magic Angle Spinning solid-state NMR (MAS-NMR) and Attenuated Total Reflectance Fourier Transform Infrared (ATR FT-IR) studies were carried out. NMR studies are performed to verify the coordination mode of the NHCs ligands on the NPs surface.[44,45] Thus, solid state $^1H–^{13}C$ cross polarization (CP) MAS-NMR spectra were recorded for bimetallic NPs stabilized with **IMes** (**Ru_2Ir@IMes** and **$RuIr_2$@IMes**) and **$IMesPrSO_3$** (**Ru_2Ir@$IMesPrSO_3$** and **$RuIr_2$@$IMesPrSO_3$**) (Figures 3, S20, S22, and S24 for **Ru_2Ir@IMes**, **$RuIr_2$@IMes**, **Ru_2Ir@$IMesPrSO_3$** and **$RuIr_2$@$IMesPrSO_3$**, respectively). In the spectra of samples stabilized by **IMes** ligand, we can observe resonance signals at 19 and 25 ppm corresponding to the methyl groups, the one at 119 ppm assigned to the imidazole backbone of the ligand, and the signals ranging from 135.0 to 127.7 ppm attributed to the aromatic zone.[46] The resonance signal of the carbenic carbon (expected at 190-200 ppm) was not observed in the spectrum which is, however, consistent with the literature due to significant peak broadening effects close to the surface (Figures 3, and S20).[44,47–50] Nevertheless, it should be noted that no signal can be observed either at the protonated position (imidazolium salt, 150 ppm), suggesting that the NHC is coordinated to the metal surface. To support this, ^1H MAS-NMR spectra were recorded on these samples (Figures S18, and S19 for **Ru_2Ir@IMes**, and **$RuIr_2$@IMes**, respectively). No signal of the proton of the carbenic carbon was detected (above 9.5 ppm). Thus, the results clearly suggest that NHC ligands are coordinated through the carbenic carbon to the surface, which may explain the high colloidal stability observed for these systems.

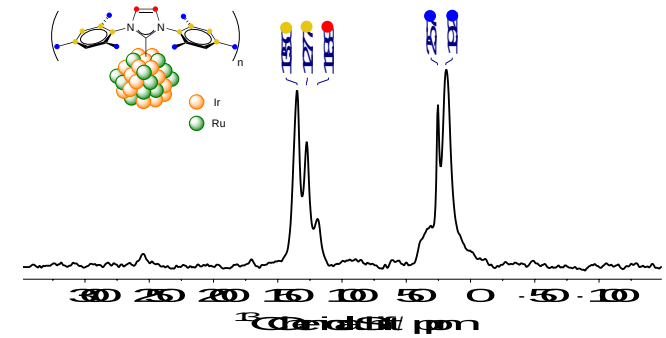

Figure 3. Solid-State ^1H-^{13}C CP MAS-NMR spectrum (125 MHz) for **Ru_2Ir@IMes**.

Likewise, water-soluble nanoparticles (**Ru_2Ir@$IMesPrSO_3$** and **$RuIr_2$@$IMesPrSO_3$**) showed similar features: i) the carbenic carbon was not observed in the $^1H–^{13}C$ CP-MAS spectra, while the signals from the methyl (overlapped with the β CH_2 group), α and γ CH_2 groups of the alkyl chain of the sulfonated N-substituent, the imidazole backbone, and the aromatic carbons resonated at 23, 48, 122, and 142 ppm, respectively (Figures S22 and S24); ii) no signal of the protonated carbenic carbon was also detected in the CP-MAS neither in the ^1H MAS spectra (Figures S21 and S23) suggesting the coordination of the hydrophilic NHC ligand to the surface.

CO adsorption experiments were carried out to evaluate the availability and accessibility of the metal atoms on the surface. CO coordinates easily on the Ru and Ir surface and displays a distinct signature according to its coordination mode and to the metal. It may coordinate in a bridging (CO_b; on the faces of the NP) or in a terminal mode (CO_t; on the apexes and edges of the NP). Thus, all NPs were exposed to CO (1 bar, r. t., 24 h) and studied by ATR-FTIR. In Figure 4, we observe the different CO adsorption bands found for all systems stabilized by **IMes**. For monometallic **Ru@IMes**, the frequencies for CO_t and CO_b are 2041, and 1968 cm^{-1}, respectively. Similarly, for **Ir@IMes** NPs, the CO_t appears at 2033 cm^{-1}. However, if we increase iridium amount in the bimetallic systems, we observe that the CO_t frequency shifts gradually to higher energies, close to the frequency of the monometallic **Ir@IMes** system (2011 and 2021 cm^{-1} for **Ru_2Ir@IMes** and **$RuIr_2$@IMes**, respectively). These results not only demonstrate that the surface of the MNPs is available for coordination of CO, which is beneficial for catalytic applications, but also suggest the presence of both metals in the same nanoparticle confirming

their bimetallic nature. Likewise, we observe the same behavior for NPs stabilized by **PVP** and **IMesPrSO$_3$** (Figures S26 and S29, respectively). It is important to highlight that the ATR-FTIR spectra recorded before adsorption of CO revealed the presence of CO on the NP surface for both **Ru@NHC** systems (Figures S27 and S28 for **Ru@IMes** and **Ru@IMesPrSO$_3$**, respectively). This behavior is typical for Ru NPs, which are able to decarbonylate the THF which was used as a solvent in the NP synthesis.[51] In contrast, for **Ru@PVP** no CO was observed before the adsorption experiment (Figure S25). It suggests an electronic effect in the decarbonylation process resulting from the electron-rich NHC ligands on the surface.[52]

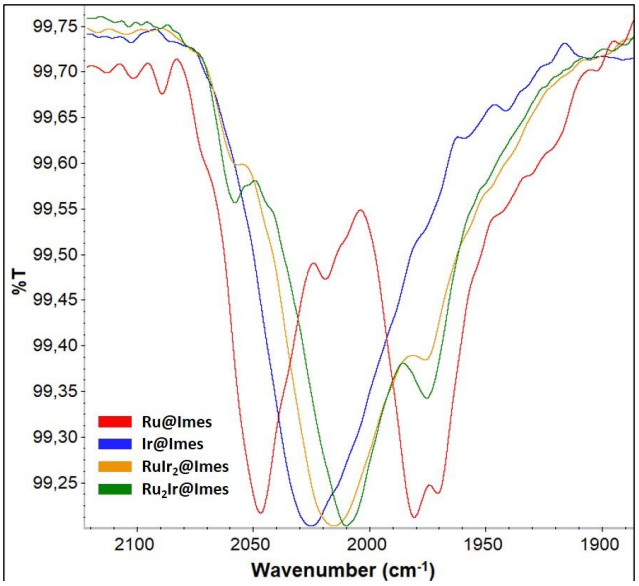

Figure 4. Infrared ATR-FTIR spectrum of NPs stabilized by **IMes** after CO adsorption. Red: **Ru@IMes**. Blue: **Ir@IMes**. Orange: **RuIr$_2$@IMes**. Green: **Ru$_2$Ir@IMes**.

Catalytic studies in Hydrogen Isotope Exchange reactions

The obtained NPs were evaluated as nanocatalysts in the HIE reactions of four different substrates with D_2 to generate a larger comparison between systems. Standard conditions chosen for these reactions were 24h at 55 °C, 2 bars of D_2, and THF as solvent as previously reported.[20,22] Initially, we selected 2-phenylpyridine as model substrate due to the possibility to evaluate selectivity of the HIE process respect to reduction of the aromatic ring by D_2. In Table 1, the experiments performed with **PVP** and **IMes**-stabilized NPs as nanocatalysts are summarized. As expected, in both systems, Ru reduced the aromatic rings (Table 1, Entries 1 and 5). Likewise, in the bimetallic system enriched in Ru and stabilized by NHCs (**Ru$_2$Ir@IMes**) the aromatic ring was also reduced, while reduction was not observed for the analogue system stabilized by **PVP** (**Ru$_2$Ir@PVP**, Table 1, Entries 6 and 2, respectively). This is attributed to an electronic effect caused by the NHC ligands on the surface which enhance the electron density and in turn the activity of the NPs towards the reduction process.[52] In contrast, Ir systems did not display reduction side process. They display a low activity towards H/D exchange in positions A and D, while, interestingly, a deuteration is observed in the remote positions B and C (Table 1, Entries 4 and 8). When bimetallic NPs were tested, an interesting effect is observed: there is a combined effect of Ru and Ir in NPs stabilized by both **PVP** and **IMes** as H/D exchange takes place in positions A, B, C, and D (Table 1, Entries 2, 3 and 7). It has been shown that Ru NPs generally display a selectivity towards positions A and D,[20] while Ir NPs deuterate positions C and B to a greater extent,[32] as it was observed in this work. Thus, this result clearly shows a synergetic effect in which the two catalytic activities of both Ru and Ir are combined and enhanced compared to their monometallic versions.[53] Additionally, a positive electronic effect from the NHC ligand is observed in the deuteration of 2-phenylpyridine being **RuIr$_2$@IMes** more active than **RuIr$_2$@PVP** (compare in Table 1 Entries 7 and 3, respectively). This is likely because NHCs are electron-rich donor ligands that may enrich electronically the surface and, hence, improve the catalytic activity of the NPs. A similar effect has been reported for NHC-stabilized Ru NPs.[52]

Table 1. H/D Exchange Reactions with 2-phenylpyridine using NPs as nanocatalysts[a]

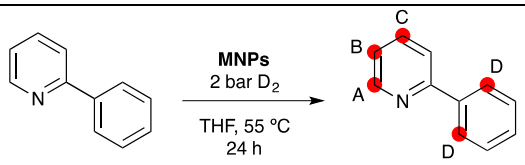

Entry	MNPs	Red[b]	Deuterium incorporation (%)[c]			
			A	B	C[d]	D
1	**Ru@PVP**	Yes[e]	--	--	--	--
2	**Ru$_2$Ir@PVP**	No[f]	68	8	14	38
3	**RuIr$_2$@PVP**	No[f]	40	29	42	16
4	**Ir@PVP**	No[f]	6	16	22	2
5	**Ru@IMes**	Yes[e]	--	--	--	--
6	**Ru$_2$Ir@IMes**	Yes[e]	--	--	--	--
7	**RuIr$_2$@IMes**	No[f]	88	81	70	85
8	**Ir@IMes**	No[f]	15	25	20	4

[a] Reaction conditions: 1 mmol of 2-phenylpyridine in the presence of 5% of NPs, 5 mL THF, 2 bar D_2, 55 °C, 24 h of reaction. [b] Reduction. [c] Determined by ^{1}H NMR. [d] Deuterium incorporation was unequivocally assigned to this position through HSQC experiment (Figure S40). [e] Reduction was not possible to be estimated due to a very complex mixture was obtained by 1H NMR spectroscopy (See Supporting Information). [f] It was estimated to be less than 5% (quantification limit of NMR).

This study was extended to two additional substrates, namely 2-methyl-naphthylamine and 5,6,7,8-tetrahydronaphthylamine using the nanoparticles stabilized by **IMes** (Table 2). Again, monometallic **Ru@IMes** and bimetallic NPs rich in Ru (**Ru$_2$Ir@IMes**) reduced the aromatic systems (Table 2, Entries 1, 2, 5, and 6). Unlike 2-phenylpyridine, in this case H/D exchange could be estimated. The corresponding A and B positions in both substrates were selectively deuterated. The position A is fa-

vored as previously described.[32] In contrast, monometallic **Ir@IMes** and bimetallic **RuIr$_2$@IMes** NPs were able to maintain the selectivity in the deuteration without appreciable reduction of the substrates (Tale 2, Entries 3, 4, 7, and 8). Additionally, when Ru is incorporated to Ir NPs, the deuteration slightly decreases at position A in both substrates (Table 2, Entries 2, 3, 6, and 7). In contrast, the deuterium incorporation at position B increases in both substrates (Table 2, compare Entries 2 and 4; and 7 and 8 for 2-methyl-naphthylamine and 5,6,7,8-tetrahydronaphthylamine, respectively). This result might suggest a slight change in selectivity for H/D exchange arising from the presence of ruthenium but is difficult to interpretate.

Finally, in order to compare the catalytic performance of the water-soluble NPs here presented with the already reported nanocatalysts for H/D exchange, we selected L-lysine as a substrate under a pH of 9.2 in D_2O (Table 3). As expected, the results showed that NPs containing Ru fully deuterated the CH_2-α, and CH_2-ε positions to the amino-acid moiety (Table 3, Entries 1, 2, and 3).[31,37] In contrast, though lower deuterations at the same positions were found using **Ir@IMesPrSO$_3$** as a catalyst (Table 3, Entry 4), no deuteration at all was observed at γ position. Interestingly, a higher deuteration degree at CH_2-γ position was observed for the bimetallic systems in comparison to the monometallic **Ru@IMesPrSO$_3$** catalyst (Table 3, compare Entries 2 and 3 to 1). The deuteration at this position is explained by bidentate coordination of the two amino groups to the NP surface. Once it occurs, the C–H bonds of the γ position point out to the surface facilitating its H/D exchange.[31] It should be noted that this transformation was reported to occur easily at pHs higher than 13, while we work here at pH of 9.2. Thus, bimetallic Ru/Ir NPs might open the possibility to perform H/D exchange of amino acids operating closer to biological conditions.

Table 2. Substrate Scope of H/D Exchange Reactions using NPs as nanocatalysts[a]

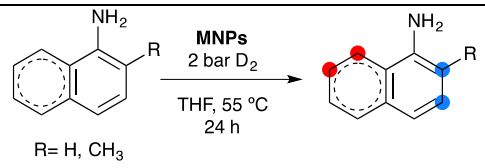

Entry	MNPs	Red(%)[b]	Product	D incorp. (%)[c] A	D incorp. (%)[c] B
1	**Ru@IMes**	84	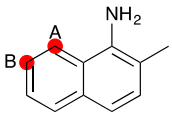	91	78
2	**Ru$_2$Ir@IMes**	48		87	16
3	**RuIr$_2$@IMes**	<5		83	8
4	**Ir@IMes**	<5		99	8
5	**Ru@IMes**	16	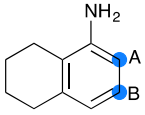	59	0
6	**Ru$_2$Ir@IMes**	10		53	6
7	**RuIr$_2$@IMes**	<5		81	22
8	**Ir@IMes**	<5		93	10

[a] Reaction conditions: 1 mmol of substrate in the presence of 5% of NPs, 5 mL THF, 2 bar D_2, 55 °C, 24 h of reaction. [b] Reduction was estimated by integrating the NMR signal of either the methyl of reduced product or the sum of the new aliphatic region in the reactions with 2-methyl-naphthylamine and 5,6,7,8-tetrahydronaphthylamine, respectively. [c] Determined by ^{1}H NMR. In the cases where reduction took place, the deuterium incorporation is given based on the NMR signals of the remaining substrate that is not reduced.

Table 3. H/D Exchange Reactions with L-Lysine using NPs as nanocatalysts[a]

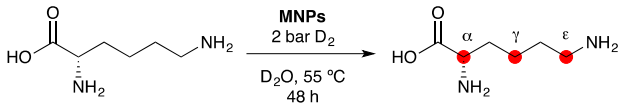

Entry	MNPs	Deuterium incorporation (%)[b] α	γ	ε
1	**Ru@IMesPrSO$_3$**	>98	14	>98
2	**Ru$_2$Ir@IMesPrSO$_3$**	>98	28	>98
3	**RuIr$_2$@IMesPrSO$_3$**	>98	27	>98
4	**Ir@IMesPrSO$_3$**	34	0	35

[a] Reaction conditions: 1 mmol of substrate in the presence of 5% of NPs, 2 mL D_2O, 2 bar D_2, 55 °C, 48 h of reaction. [b] Determined by ^{1}H NMR.

CONCLUSIONS

In summary, we report here a facile synthesis and full characterization of new lipo- and water-soluble bimetallic Ru/Ir NPs stabilized by NHC ligands. The bimetallic nature of the NPs was confirmed by HR-STEM coupled to EDX as well as by ATR-FTIR after reaction with CO. Furthermore, the coordination of the NHCs to the NP surface was suggested by solid state NMR. This coordination explains the high colloidal stability observed for all the NPs here reported. To the best of our knowledge, this is the first report of bimetallic Ru/Ir NPs that were employed in H/D exchange reactions. Interestingly, these NPs exhibited high activity towards aromatic N-containing substrates such as 2-phenylpyridine, 2-methyl-naphthylamine and 5,6,7,8-tetrahydronaphthylamine. Important features emerge from our catalytic results: i) ruthenium-rich NPs are able to reduce aromatic rings whereas iridium rich NPs cannot; ii) a synergetic effect is observed when **RuIr$_2$** NPs were used as catalysts, suppressing the reduction process, and enhancing the activity of each metal while their selectivity in H/D exchange is preserved; and iii) the presence of NHC ligands on the surface of the NPs induces a positive electronic effect on their catalytic activity compared to their counterparts stabilized by PVP. Finally, the reactivity towards deuteration of L-lysine presented similar values regardless of the nature of the NP. Nevertheless, it was found that iridium improves the selectivity towards γ position under milder pH conditions (9.2 Vs. 13). These systems are therefore promising nanocatalysts that may operate under biological conditions using bioactive molecules.

ASSOCIATED CONTENT

Supporting Information

The Supporting Information is available free of charge on the ACS Publications website. Experimental section, TEM, XRD, ATR-FTIR, and solid-state NMR spectra of the NPs obtained, as well as solution NMR spectra of the catalytic studies.

AUTHOR INFORMATION

Corresponding Author

*E-mail: menciabe@insa-toulouse.fr (G.M.), chaudret@insa-toulouse.fr (B.C.), and eabaquerov@unal.edu.co (E.A.B.)

Current Address

† IFP Energies nouvelles, Rond-point de l'échangeur de Solaize, BP 3, 69360 Solaize, France.

Notes

The authors declare no competing financial interests.

ACKNOWLEDGMENT

This work was supported by the Universidad Nacional de Colombia (Project with HERMES code 48530), H2020/FET-Open FLIX-862179, ERC-AdG MONACAT No. 694159. A. Z. V. is grateful to NanoX Graduate School of Research program for her internship at LPCNO in Toulouse. We thank Y. Coppel for Solid-State NMR measurements.

Dedicated to Professor Maurice Brookhart, an outstanding chemist and a great friend on his 80th birthday.

REFERENCES

(1) Brookhart, M.; Green, M. L. H. Carbon-Hydrogen-Transition Metal Bonds. *J. Organomet. Chem.* **1983**, *250* (1), 395–408. https://doi.org/10.1016/0022-328X(83)85065-7.

(2) Brookhart, M.; Green, M. L. H.; Parkin, G. Agostic Interactions in Transition Metal Compounds. *Proc. Natl. Acad. Sci.* **2007**, *104* (17), 6908–6914. https://doi.org/10.1073/pnas.0610747104.

(3) Brookhart, M.; Green, M. L. H.; Wong, L.-L. Carbon-Hydrogen-Transition Metal Bonds; 2007; pp 1–124. https://doi.org/10.1002/9780470166376.ch1.

(4) Atzrodt, J.; Derdau, V.; Kerr, W. J.; Reid, M. Deuterium- and Tritium-Labelled Compounds: Applications in the Life Sciences. *Angew. Chem. Int. Ed.* **2018**, *57* (7), 1758–1784. https://doi.org/10.1002/anie.201704146.

(5) Katsnelson, A. Heavy Drugs Draw Heavy Interest from Pharma Backers. *Nat. Med.* **2013**, *19* (6), 656–656. https://doi.org/10.1038/nm0613-656.

(6) Pirali, T.; Serafini, M.; Cargnin, S.; Genazzani, A. A. Applications of Deuterium in Medicinal Chemistry. *J. Med. Chem.* **2019**, *62* (11), 5276–5297. https://doi.org/10.1021/acs.jmedchem.8b01808.

(7) Kopf, S.; Bourriquen, F.; Li, W.; Neumann, H.; Junge, K.; Beller, M. Recent Developments for the Deuterium and Tritium Labeling of Organic Molecules. *Chem. Rev.* **2022**, *122* (6), 6634–6718. https://doi.org/10.1021/acs.chemrev.1c00795.

(8) Atzrodt, J.; Derdau, V. Pd- and Pt-Catalyzed H/D Exchange Methods and Their Application for Internal MS Standard Preparation from a Sanofi-Aventis Perspective. *J. Label. Compd. Radiopharm.* **2010**, *53* (11–12), 674–685. https://doi.org/10.1002/jlcr.1818.

(9) Reid, M. Iridium Catalysts for Hydrogen Isotope Exchange; 2020; pp 271–302. https://doi.org/10.1007/3418_2020_58.

(10) Hesk, D. Highlights of C (Sp^2)-H Hydrogen Isotope Exchange Reactions. *J. Label. Compd. Radiopharm.* **2020**, *63* (6), 247–265. https://doi.org/10.1002/jlcr.3801.

(11) Valero, M.; Derdau, V. Highlights of Aliphatic C(Sp3)-H Hydrogen Isotope Exchange Reactions. *J. Label. Compd. Radiopharm.* **2020**, *63* (6), 266–280. https://doi.org/10.1002/jlcr.3783.

(12) Rhinehart, J. L.; Manbeck, K. A.; Buzak, S. K.; Lippa, G. M.; Brennessel, W. W.; Goldberg, K. I.; Jones, W. D. Catalytic Arene H/D Exchange with Novel Rhodium and Iridium Complexes. *Organometallics* **2012**, *31* (5), 1943–1952. https://doi.org/10.1021/om2012419.

(13) Kang, Q.; Li, Y.; Chen, K.; Zhu, H.; Wu, W.; Lin, Y.; Shi, H. Rhodium-Catalyzed Stereoselective Deuteration of Benzylic C–H Bonds via Reversible η 6 -Coordination. *Angew. Chem. Int. Ed.* **2022**, *61* (11). https://doi.org/10.1002/anie.202117381.

(14) Yang, H.; Hesk, D. Base Metal-Catalyzed Hydrogen Isotope Exchange. *J. Label. Compd. Radiopharm.* **2020**, *63* (6), 296–307. https://doi.org/10.1002/jlcr.3826.

(15) Zarate, C.; Yang, H.; Bezdek, M. J.; Hesk, D.; Chirik, P. J. Ni(I)–X Complexes Bearing a Bulky α-Diimine Ligand: Synthesis, Structure, and Superior Catalytic Performance in the Hydrogen Isotope Exchange in Pharmaceuticals. *J. Am. Chem. Soc.* **2019**, *141* (12), 5034–5044. https://doi.org/10.1021/jacs.9b00939.

(16) Hesk, D.; Lavey, C. F.; McNamara, P. Tritium Labelling of Pharmaceuticals by Metal-Catalysed Exchange Methods. *J. Label. Compd. Radiopharm.* **2010**, *53* (11–12), 722–730. https://doi.org/10.1002/jlcr.1800.

(17) Heys, J. R. Nickel-Catalyzed Hydrogen Isotope Exchange. *J. Label. Compd. Radiopharm.* **2010**, *53* (11–12), 716–721. https://doi.org/10.1002/jlcr.1822.

(18) Lepron, M.; Daniel-Bertrand, M.; Mencia, G.; Chaudret, B.; Feuillastre, S.; Pieters, G. Nanocatalyzed Hydrogen Isotope Exchange. *Acc. Chem. Res.* **2021**, *54* (6), 1465–1480. https://doi.org/10.1021/acs.accounts.0c00721.

(19) Leeuwen, P. W. N. M. Van; Claver, C. *Recent Advances in Nanoparticle Catalysis*; van Leeuwen, P. W. N. M., Claver, C., Eds.; Molecular Catalysis; Springer International Publishing: Cham, 2020; Vol. 1. https://doi.org/10.1007/978-3-030-45823-2.

(20) Pieters, G.; Taglang, C.; Bonnefille, E.; Gutmann, T.; Puente, C.; Berthet, J.-C.; Dugave, C.; Chaudret, B.; Rousseau, B. Regioselective and Stereospecific Deuteration of Bioactive Aza Compounds by the Use of Ruthenium Nanoparticles. *Angew. Chem. Int. Ed.* **2014**, *53* (1), 230–234. https://doi.org/10.1002/anie.201307930.

(21) Gao, L.; Perato, S.; Garcia-Argote, S.; Taglang, C.; Martínez-Prieto, L. M.; Chollet, C.; Buisson, D. A.; Dauvois, V.; Lesot, P.; Chaudret, B.; Rousseau, B.; Feuillastre, S.; Pieters, G. Ruthenium-Catalyzed Hydrogen Isotope Exchange of C(Sp3)-H Bonds Directed by a Sulfur Atom. *Chem. Commun.* **2018**, *54* (24), 2986–2989. https://doi.org/10.1039/c8cc00653a.

(22) Taglang, C.; Martínez-Prieto, L. M.; del Rosal, I.; Maron, L.; Poteau, R.; Philippot, K.; Chaudret, B.; Perato, S.; Sam Lone, A.; Puente, C.; Dugave, C.; Rousseau, B.; Pieters, G. Enantiospecific C□H Activation Using Ruthenium Nanocatalysts. *Angew. Chem. Int. Ed.* **2015**, *54* (36), 10474–10477. https://doi.org/10.1002/anie.201504554.

(23) Reshi, N. U. D.; Samuelson, A. G. Recent Advances in Soluble Ruthenium(0) Nanocatalysts and Their Reactivity. *Appl. Catal. A Gen.* **2020**, *598*, 117561. https://doi.org/10.1016/j.apcata.2020.117561.

(24) Martínez-Prieto, L. M.; Chaudret, B. Organometallic Ruthenium Nanoparticles: Synthesis, Surface Chemistry, and Insights into Ligand Coordination. *Acc. Chem. Res.* **2018**, *51* (2), 376–384. https://doi.org/10.1021/acs.accounts.7b00378.

(25) Heuer-Jungemann, A.; Feliu, N.; Bakaimi, I.; Hamaly, M.; Alkilany, A.; Chakraborty, I.; Masood, A.; Casula, M. F.; Kostopoulou, A.; Oh, E.; Susumu, K.; Stewart, M. H.; Medintz, I. L.; Stratakis, E.; Parak, W. J.; Kanaras, A. G. The Role of Ligands in the Chemical Synthesis and Applications of Inorganic Nanoparticles. *Chem. Rev.* **2019**, *119* (8), 4819–4880. https://doi.org/10.1021/acs.chemrev.8b00733.

(26) Zhukhovitskiy, A. V.; MacLeod, M. J.; Johnson, J. A. Carbene Ligands in Surface Chemistry: From Stabilization of Discrete Elemental Allotropes to Modification of Nanoscale and Bulk Substrates. *Chem. Rev.* **2015**, *115* (20), 11503–11532. https://doi.org/10.1021/acs.chemrev.5b00220.

(27) Smith, C. A.; Narouz, M. R.; Lummis, P. A.; Singh, I.; Nazemi,

A.; Li, C. H.; Crudden, C. M. N-Heterocyclic Carbenes in Materials Chemistry. *Chem. Rev.* **2019**, *119* (8), 4986–5056. https://doi.org/10.1021/acs.chemrev.8b00514.

(28) Shen, H.; Tian, G.; Xu, Z.; Wang, L.; Wu, Q.; Zhang, Y.; Teo, B. K.; Zheng, N. N-Heterocyclic Carbene Coordinated Metal Nanoparticles and Nanoclusters. *Coord. Chem. Rev.* **2022**, *458*, 214425. https://doi.org/10.1016/j.ccr.2022.214425.

(29) Koy, M.; Bellotti, P.; Das, M.; Glorius, F. N-Heterocyclic Carbenes as Tunable Ligands for Catalytic Metal Surfaces. *Nat. Catal.* **2021**, *4* (5), 352–363. https://doi.org/10.1038/s41929-021-00607-z.

(30) An, Y. Y.; Yu, J. G.; Han, Y. F. Recent Advances in the Chemistry of N-Heterocyclic-Carbene-Functionalized Metal-Nanoparticles and Their Applications. *Chinese J. Chem.* **2019**, *37* (1), 76–87. https://doi.org/10.1002/cjoc.201800450.

(31) Martínez-Prieto, L. M.; Baquero, E. A.; Pieters, G.; Flores, J. C.; De Jesús, E.; Nayral, C.; Delpech, F.; Van Leeuwen, P. W. N. M.; Lippens, G.; Chaudret, B. Monitoring of Nanoparticle Reactivity in Solution: Interaction of l-Lysine and Ru Nanoparticles Probed by Chemical Shift Perturbation Parallels Regioselective H/D Exchange. *Chem. Commun.* **2017**, *53* (43), 5850–5853. https://doi.org/10.1039/c7cc02445b.

(32) Valero, M.; Bouzouita, D.; Palazzolo, A.; Atzrodt, J.; Dugave, C.; Tricard, S.; Feuillastre, S.; Pieters, G.; Chaudret, B.; Derdau, V. NHC-Stabilized Iridium Nanoparticles as Catalysts in Hydrogen Isotope Exchange Reactions of Anilines. *Angew. Chem. Int. Ed.* **2020**, *59* (9), 3517–3522. https://doi.org/10.1002/anie.201914369.

(33) Pan, C.; Dassenoy, F.; Casanove, M.-J.; Philippot, K.; Amiens, C.; Lecante, P.; Mosset, A.; Chaudret, B. A New Synthetic Method toward Bimetallic Ruthenium Platinum Nanoparticles; Composition Induced Structural Changes. *J. Phys. Chem. B* **1999**, *103* (46), 10098–10101. https://doi.org/10.1021/jp992072m.

(34) Dassenoy, F.; Casanove, M.-J.; Lecante, P.; Pan, C.; Philippot, K.; Amiens, C.; Chaudret, B. Size and Composition Effects in Polymer-Protected Ultrafine Bimetallic Pt_xRu_{1-x} ($0 < x < 1$) Particles. *Phys. Rev. B* **2001**, *63* (23), 235407. https://doi.org/10.1103/PhysRevB.63.235407.

(35) Lara, P.; Casanove, M.-J.; Lecante, P.; Fazzini, P.-F.; Philippot, K.; Chaudret, B. Segregation at a Small Scale: Synthesis of Core–Shell Bimetallic RuPt Nanoparticles, Characterization and Solid State NMR Studies. *J. Mater. Chem.* **2012**, *22* (8), 3578. https://doi.org/10.1039/c2jm14757b.

(36) Lara, P.; Ayvalı, T.; Casanove, M.-J.; Lecante, P.; Mayoral, A.; Fazzini, P.-F.; Philippot, K.; Chaudret, B. On the Influence of Diphosphine Ligands on the Chemical Order in Small RuPt Nanoparticles: Combined Structural and Surface Reactivity Studies. *Dalton. Trans.* **2013**, *42* (2), 372–382. https://doi.org/10.1039/C2DT31646C.

(37) Bouzouita, D.; Lippens, G.; Baquero, E. A.; Fazzini, P. F.; Pieters, G.; Coppel, Y.; Lecante, P.; Tricard, S.; Martínez-Prieto, L. M.; Chaudret, B. Tuning the Catalytic Activity and Selectivity of Water-Soluble Bimetallic RuPt Nanoparticles by Modifying Their Surface Metal Distribution. *Nanoscale* **2019**, *11* (35), 16544–16552. https://doi.org/10.1039/c9nr04149d.

(38) Saadun, A. J.; Mitchell, S.; Bonchev, H.; Pérez-Ramírez, J. Carbon-Supported Bimetallic Ruthenium-Iridium Catalysts for Selective and Stable Hydrodebromination of Dibromomethane. *ChemCatChem* **2022**, *14* (2), e2021014. https://doi.org/10.1002/cctc.202101494.

(39) Chimentão, R. J.; Oliva, H.; Russo, V.; Llorca, J.; Fierro, J. L. G.; Mäki-Arvela, P.; Murzin, D. Y.; Ruiz, D. Catalytic Transformation of Biomass-Derived 5-Hydroxymethylfurfural over Supported Bimetallic Iridium-Based Catalysts. *J. Phys. Chem. C* **2021**, *125* (18), 9657–9678. https://doi.org/10.1021/acs.jpcc.1c00958.

(40) Wang, J.; Zhu, S.; Wang, Y.; Wang, Y.; Jin, G.; Tong, X.; Guo, X. Enhanced Activity of Ru-Ir Nanoparticles over SiC for Hydrogenation of Levulinic Acid at Room-Temperature. *Mater. Res. Bull.* **2021**, *135*, 111128. https://doi.org/10.1016/j.materresbull.2020.111128.

(41) You, Y.-W.; Kim, Y. J.; Lee, J. H.; Arshad, M. W.; Kim, S. K.; Kim, S. M.; Lee, H.; Thompson, L. T.; Heo, I. Unraveling the Origin of Extraordinary Lean NOx Reduction by CO over Ir-Ru Bimetallic Catalyst at Low Temperature. *Appl. Catal. B Environ.* **2021**, *280*, 119374. https://doi.org/10.1016/j.apcatb.2020.119374.

(42) Danilovic, N.; Subbaraman, R.; Chang, K. C.; Chang, S. H.; Kang, Y.; Snyder, J.; Paulikas, A. P.; Strmcnik, D.; Kim, Y. T.; Myers, D.; Stamenkovic, V. R.; Markovic, N. M. Using Surface Segregation To Design Stable Ru-Ir Oxides for the Oxygen Evolution Reaction in Acidic Environments. *Angew. Chem. Int. Ed.* **2014**, *53* (51), 14016–14021. https://doi.org/10.1002/anie.201406455.

(43) Clayton, K. N.; Salameh, J. W.; Wereley, S. T.; Kinzer-Ursem, T. L. Physical Characterization of Nanoparticle Size and Surface Modification Using Particle Scattering Diffusometry. *Biomicrofluidics* **2016**, *10* (5), 054107. https://doi.org/10.1063/1.4962992.

(44) Baquero, E. A.; Tricard, S.; Flores, J. C.; de Jesús, E.; Chaudret, B. Highly Stable Water-Soluble Platinum Nanoparticles Stabilized by Hydrophilic N-Heterocyclic Carbenes. *Angew. Chem. Int. Ed.* **2014**, *53* (48), 13220–13224. https://doi.org/10.1002/anie.201407758.

(45) Asensio, J. M.; Tricard, S.; Coppel, Y.; Andrés, R.; Chaudret, B.; de Jesús, E. Knight Shift in 13 C NMR Resonances Confirms the Coordination of N-Heterocyclic Carbene Ligands to Water-Soluble Palladium Nanoparticles. *Angew. Chem. Int. Ed.* **2017**, *56* (3), 865–869. https://doi.org/10.1002/anie.201610251.

(46) Ernst, J. B.; Muratsugu, S.; Wang, F.; Tada, M.; Glorius, F. Tunable Heterogeneous Catalysis: N-Heterocyclic Carbenes as Ligands for Supported Heterogeneous Ru/K-Al 2 O 3 Catalysts To Tune Reactivity and Selectivity. *J. Am. Chem. Soc.* **2016**, *138* (34), 10718–10721. https://doi.org/10.1021/jacs.6b03821.

(47) Lara, P.; Rivada-Wheelaghan, O.; Conejero, S.; Poteau, R.; Philippot, K.; Chaudret, B. Ruthenium Nanoparticles Stabilized by N-Heterocyclic Carbenes: Ligand Location and Influence on Reactivity. *Angew. Chem. Int. Ed.* **2011**, *50* (50), 12080–12084. https://doi.org/10.1002/anie.201106348.

(48) Gonzalez-Galvez, D.; Lara, P.; Rivada-Wheelaghan, O.; Conejero, S.; Chaudret, B.; Philippot, K.; Van Leeuwen, P. W. N. M. NHC-Stabilized Ruthenium Nanoparticles as New Catalysts for the Hydrogenation of Aromatics. *Catal. Sci. Technol.* **2013**, *3* (1), 99–105. https://doi.org/10.1039/c2cy20561k.

(49) Lara, P.; Suárez, A.; Collière, V.; Philippot, K.; Chaudret, B. Platinum N-Heterocyclic Carbene Nanoparticles as New and Effective Catalysts for the Selective Hydrogenation of Nitroaromatics. *ChemCatChem* **2014**, *6* (1), 87–90. https://doi.org/10.1002/cctc.201300821.

(50) Pan, C.; Pelzer, K.; Philippot, K.; Chaudret, B.; Dassenoy, F.; Lecante, P.; Casanove, M.-J. Ligand-Stabilized Ruthenium Nanoparticles: Synthesis, Organization, and Dynamics. *J. Am. Chem. Soc.* **2001**, *123* (31), 7584–7593. https://doi.org/10.1021/ja003961m.

(51) Martínez-Prieto, L. M.; Urbaneja, C.; Palma, P.; Cámpora, J.; Philippot, K.; Chaudret, B. A Betaine Adduct of N-Heterocyclic Carbene and Carbodiimide, an Efficient Ligand to Produce Ultra-Small Ruthenium Nanoparticles. *Chem. Commun.* **2015**, *51* (22), 4647–4650. https://doi.org/10.1039/C5CC00211G.

(52) Martínez-Prieto, L. M.; van Leeuwen, P. W. N. M. Ligand Effects in Ruthenium Nanoparticle Catalysis; 2020; pp 407–448. https://doi.org/10.1007/978-3-030-45823-2_12.

(53) Singh, A. K.; Xu, Q. Synergistic Catalysis over Bimetallic Alloy Nanoparticles. *ChemCatChem* **2013**, *5* (3), 652–676. https://doi.org/10.1002/cctc.201200591.

TOC Graphic

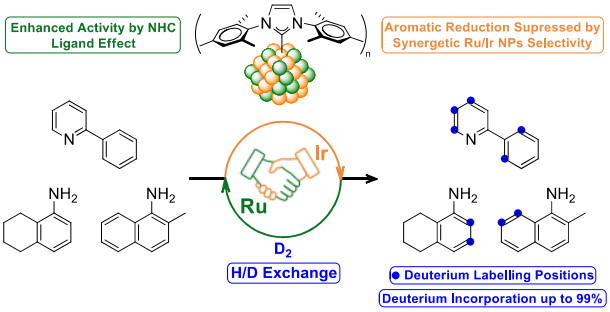
Enhanced Activity by NHC Ligand Effect
Aromatic Reduction Supressed by Synergetic Ru/Ir NPs Selectivity
N
N
n
NH2
NH2
Ir
Ru
D2
H/D Exchange
NH2
NH2
Deuterium Labelling Positions
Deuterium Incorporation up to 99%